BECKMAN COULTER
Life Sciences

Demystifying DGE-AUC Part 5: Optimizing data quality

Akash Bhattacharya
Beckman Coulter Life Sciences, 4510 Byrd Dr, Loveland, CO 80538

Abstract

In this application note, we discuss the optimization of Density Gradient Equilibrium Analytical Ultracentrifugation (DGE-AUC) to obtain superior data quality. There are several experimental parameters which can be adjusted. In this study, we will explore the effects of adjusting rotor speed, temperature, gradient-forming materials (GFM) starting density and absorbance wavelength. Our results are based on a sample of Adeno-Associated Virus Serotype 9 or AAV9 in CsCl/PBS buffer. DGE-AUC data is easily visually interpreted. Therefore, the optimization will largely be based upon visual inspection of data. In some cases, the effect of optimization will also be demonstrated via DGE peak analysis performed using the Origin software package.

Introduction

We started part 1 this technical series (Demystifying DGE-AUC Part 1: Back to the Basics) by describing Analytical Ultracentrifugation (AUC) as a versatile technique for quantitative characterization of the biophysical properties of analytes in solution[1]. Advancements in instrumentation allowed the AUC to be applied to research problems in a wide range of biophysical systems. The intent behind this series is to provide insights into Density Gradient Equilibrium Analytical Ultracentrifugation (DGE-AUC). AUC hardware has come a very long way from the seminal Meselson and Stahl experiments of 1958[2], which can
be considered the progenitor of the modern DGE-AUC method. It remains a truism, however, that optimizing the experimental protocol yields better and more easily interpretable data. Demonstrating this is the purpose behind this installment of this technical series.

Background

In part 2 of this technical series (Demystifying DGE-AUC Part 2: Physical Principles and Links to Preparative DGUC), we have discussed the selection criterion for gradient-forming materials (GFMs). We assume that the starting point for discussion in this technical note is when we already have a sample ready for experiment which includes a target analyte (in this case Adeno-Associated Virus[3-5] Serotype 9 or AAV9), a suitable buffer (in this case PBS at pH 7.4) and a suitable GFM (in this case CsCl). Thus, all of the biochemistry pre-work which goes into sample preparation is completed and there are no outstanding concerns about sample and GFM compatibility or sample stability.

Part 3 of this technical series (Demystifying DGE-AUC Part 3: Sample Preparation) explained the concept of preparing the DGE-AUC samples to reach a target density, demonstrated the use of a sample preparation spreadsheet calculator. That spreadsheet calculator was used to prepare the AAV9 samples used in this study. Part 4 of this series (Demystifying DGE-AUC Part 4: Fundamentals of Data Analysis) demonstrated data analysis for experiments carried out with the AAV9 samples mentioned above using the popular software package Origin.

This application note is the fifth in this series and will discuss the optimization of DGE-AUC experiments in the modern Optima AUC using this sample of AAV9. The subsequent results section will show absorption data pertaining to the analyte. This application note will not delve into the corresponding Rayleigh Interference Fringe (RIF) data which shows the formation of the CsCl gradient, since that topic has been explored in part II of this series.

About the experiment

This application note deals with DGE-AUC experiments conducted on a sample of AAV9 with absorbance detection at multiple wavelengths. There are several aspects of the experiment which can be optimized. These can be broadly classified as follows:

Sample parameters

- Sample / analyte concentration
- GFM starting concentration / density
- Buffering agent
- Buffer pH
- Salt concentration
- Buffer Additives (such as reducing agents)
- Stabilizing agents (such as glycerol)

Centrifuge parameters

- Rotor speed
- Temperature
- Absorbance wavelength

In this study, we will principally deal with GFM starting concentration, rotor speed, temperature and wavelength. In general, it is advisable to optimize parameters related to sample biochemistry (such as buffer, pH, etc) at the outset and then move on to GFM starting concentration and then finally to the centrifuge parameters.

Sample Information

The following results in method optimization were carried out on a sample of Adeno-Associated Virus (AAV) in CsCl based buffer. The specific sample conditions were as follows:

Sample #	Analyte	GFM	GFM starting density	Buffer
1	AAV9	CsCl	1.37 g/mL	PBS, pH 7.4
2	AAV9	CsCl	1.35 g/mL	PBS, pH 7.4
3	AAV9	CsCl	1.33 g/mL	PBS, pH 7.4

Table 1: Sample information

Some of the experiments discussed in the subsequent sections pertain to only one specific starting concentration of CsCl – 1.35 g/ml.

Experimental parameters

The different optimization steps were largely extracted from a multiwavelength, multispeed experiments. Two such experiments were carried out on the samples outlined in Table 1 – at 20°C and 4°C. Relevant data acquisition parameters are shown below:

Stage	Rotor speed (krpm)	Wavelengths (nm)	Scans/Wavelength	Scan Interval (min)
1	7	230, 260, 280	100	5
2	14	"	100	5
3	21	"	100	5
4	28	"	100	5
5	35	"	100	5
6	42	"	100	5

Figure 2: Experimental parameters

DGE-AUC Method optimization

Morphology of experimental DGE-AUC absorbance data for an analyte

Before we discuss the optimization of DGE-AUC data, it is desirable to understand the features of a DGE-AUC absorbance scan. In Figure 1, the following features of a DGE-AUC absorbance scan recorded at 230 nm for a sample of AAV9 in 1.35 g/ml CsCl in PBS are shown. The air gap region is boxed in cyan, the meniscus region in orange, the density gradient region, which will be used for analysis is boxed in grey, while the cell bottom region is boxed in maroon. It is only the region boxed in grey – i.e. the density gradient region that will be used for data analysis.

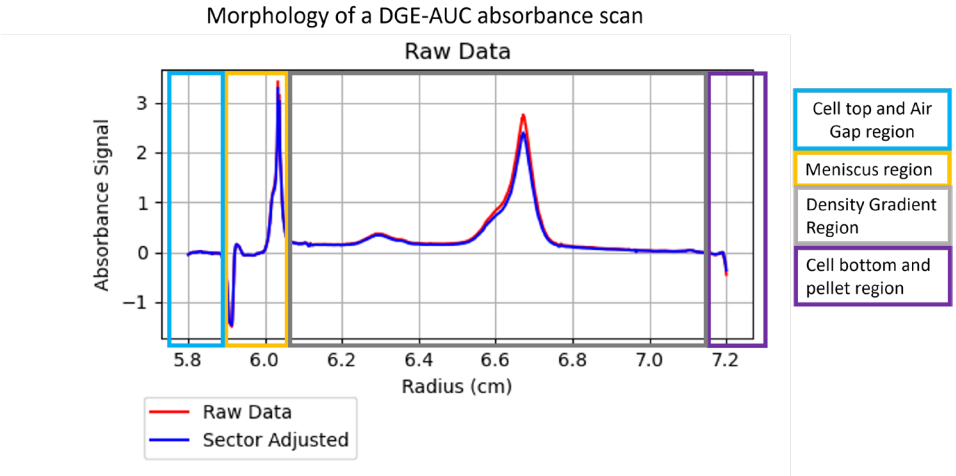

Figure 1: Morphology of an absorbance scan dataset for DGE-AUC of AAV in CsCl

Understanding optimization of DGE-AUC

The following sections will cover optimization of DGE-AUC scans by adjusting various input parameters. Therefore, it is apposite to discuss what an optimized DGE-AUC scan might look like. The following Figure 2 shows the DGE-AUC peaks obtained for a hypothetical sample containing only one analyte particle with a buoyant density of 1.2 g/ml in a buffer containing CsCl GFM.

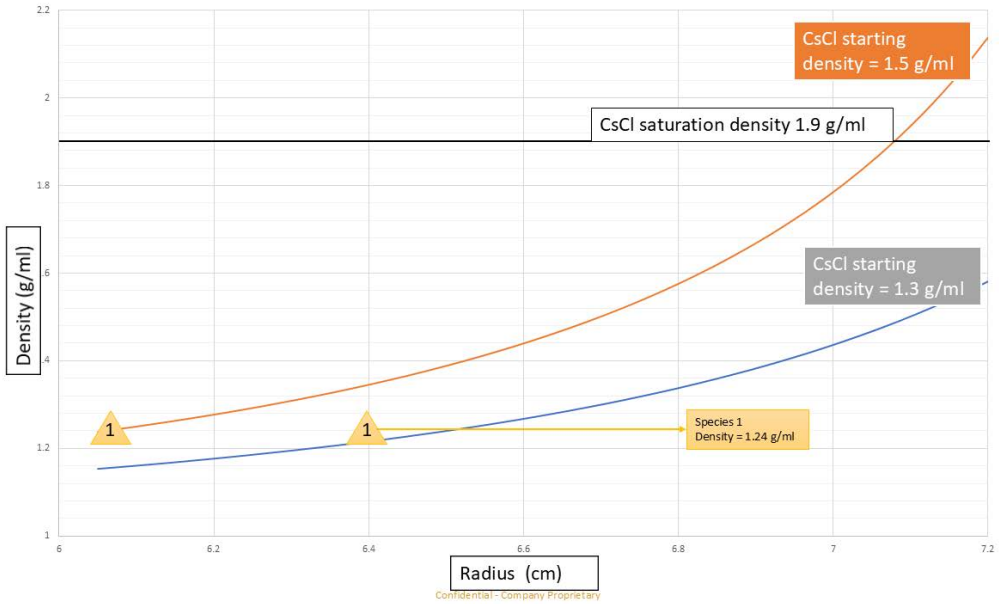

Figure 2: The effect of changing GFM starting concentration on DGE-AUC peaks

This hypothetical experiment was run at 50000 rpm. In this figure, the blue trace shows the GFM density gradient when the starting density of CsCl is 1.3 g/ml. The density gradient exists from the meniscus, which is at 6.05 cm to the cell bottom, which is at 7.2 cm. It has been shown in part II of this technical series that the density gradient forms by pivoting around a specific radial positon where the equilibrium density is the same as the uniform starting density (in this case 1.3 g/ml). This point is called the "isodensity point". At equilibrium, the analyte accumulates as a band at the radial position corresponding to its own buoyant density. In this case, this occurs at 6.35 cm, as represented by the yellow triangle intersecting the blue GFM trace. Now, if the starting density of CsCl was 1.5 g/ml, instead of 1.3 g/ml, then two problems occur. The first is that at this rotor speed, the density of CsCl will attain its saturation value at a radial position of around 7.08 cm and begin to precipitate. This can cause instrument damage. Therefore, in practice care should be taken to avoid reaching the saturation density of the GFM. This is one of the reasons why simulating density gradients prior to experiments is recommended whenever possible. The second problem is that the lowest density attained by the GFM is 1.238 g/ml. This is higher than the buoyant density of analyte 1. Thus, analyte 1 will float to the top of the AUC sample cell and accumulate at the meniscus, as shown in Figure 2 with the yellow triangle at a radial position of 6.05 cm. This makes quantification of analyte 1 difficult. Thus, this figure shows the importance of selecting the correct GFM starting density. Too high a value will ensure that the analyte floats upwards to the meniscus since its buoyant density is lower than the lowest value captured by the density gradient dynamic range (at a given speed). Not shown in Figure 2 is the effect of starting with too low a value of GFM density. This situation is the obverse of that depicted herein. In such an example, the analyte buoyant density might be greater than the highest lowest value captured by the density gradient dynamic range (at a given speed) – leading to the analyte pelleting at the bottom of the cell.

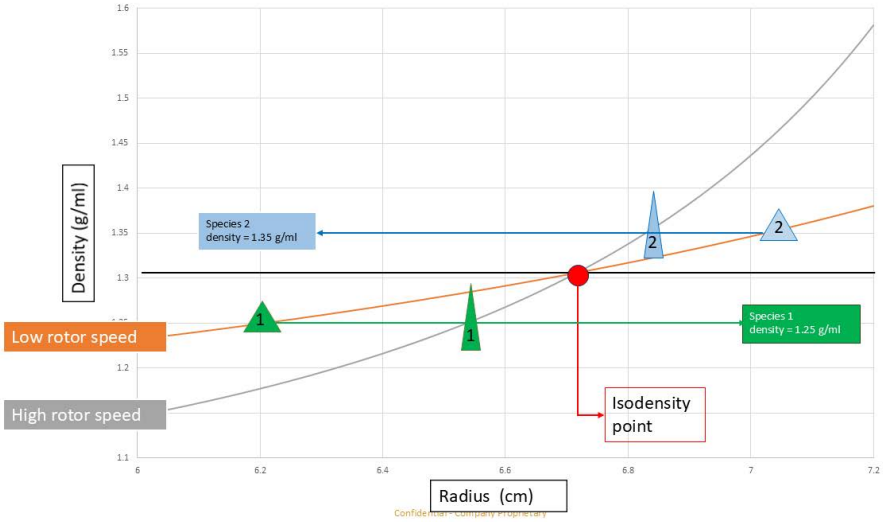

Figure 3: The effect of changing rotor speed on DGE-AUC peaks

The previous example in Figure 2 showed the effect of changing GFM starting density at a constant rotor speed. This example in Figure 3 shows the effect of changing rotor speed with a constant GFM starting density. This example refers to a hypothetical sample with two analytes: Analyte 1 with a buoyant density of 1.25 g/ml and Analyte 2 with a buoyant density of 1.35 g/ml. The GFM is CsCl at a starting density of 1.3 g/ml. At a low rotor speed (30000 rpm), the GFM forms a density gradient shown by the orange trace. At a high rotor speed (50000 rpm), the GFM forms a steeper density gradient shown by the grey trace. In this example, the GFM starting density is chosen to be 1.3 g/ml, which is midway between the buoyant densities of Analytes 1 and 2.

When the experiment is conducted at the lower rotor speed (orange trace, 30000 rpm), the position of Analyte 1 is at ~6.2 cm as shown by the broad green triangle (representing a broad and shallow peak). Analyte 2 is located at ~7.02 cm as shown by the broad light blue triangle (representing a broad and shallow peak).

When the experiment is conducted at the higher rotor speed (grey trace, 50000 rpm), the position of Analyte 1 shifts to ~6.54 cm as shown by the narrow green triangle (representing a narrow and high peak). Analyte 2 shifts to ~6.83 cm as shown by the narrow light blue triangle (representing a narrow and high peak).

Thus, the following observations can be made:

1. The two peaks corresponding to Analytes 1 and 2 are on opposite sides of the isodensity point. This is not by accident. The GFM starting concentration (here 1.3 g/ml) is chosen to ensure this. Ideally, the isodensity point should be in the middle of the entire density distribution range corresponding to all analytes in the sample.

2. At lower rotor speeds, the peaks corresponding to Analytes 1 and 2 are more widely separated. At higher rotor speeds, the peaks shift inward towards the isodensity point.

3. At lower rotor speeds, the peaks are broader and shallower. At higher rotor speeds, the peaks are narrower and taller.

4. Thus, lower rotor speeds provide better separation between peak centers corresponding to the two analytes. However, higher rotor speeds provide better S/N ratio. This is an unavoidable experimental tradeoff.

Summing up, optimizing a DGE-AUC experiment has the following objectives:

1. Ensure that DGE peaks corresponding to all analytes fall within the dynamic range of the density gradient.

2. Obtain a balance between peak separation and peak height so that individual DGE-AUC peaks can be integrated, and sample populations can be quantified.

Results

In the following sections, we will discuss the effect of optimizing rotor speed, GFM starting density, temperature and selecting the correct detection wavelengths.

Rotor Speed Optimization

Figure 4 shows the effect of rotor speed on DGE-AUC absorption data recorded for AAV9 in 1.35 g/ml CsCl with PBS buffer at pH 7.4. Experiment conditions were as follows: absorption scans at 260 nm were collected at intervals of 5 minutes at a temperature of 20°C. This was a speedstep (aka multispeed) experiment, with 100 scans each collected at successive rotor speeds, allowing equilibrium to be attained at each step. DGE peaks start appearing only at 28 krpm, as seen in panel D. At 28 krpm, it is as yet, not possible to determine the number of peaks by visual inspection. At 35 krpm (panel E), two distinct peaks are seen, a major peak at 6.7 cm, and a minor peak at 6.1 cm. However, the minor peak is very close to the meniscus. This illustrates the point raised in the preceding section – higher rotor speeds are needed to extend the dynamic range of densities to sample all the species in the sample. This does happen at 42 krpm, wherein the minority peak accumulates at 6.3 cm (panel F). Interestingly enough, it is now also apparent that the main peak at ~ 6.7 cm has a left shoulder peak indicating a sub-population with a slightly lower buoyant density within the main peak species.

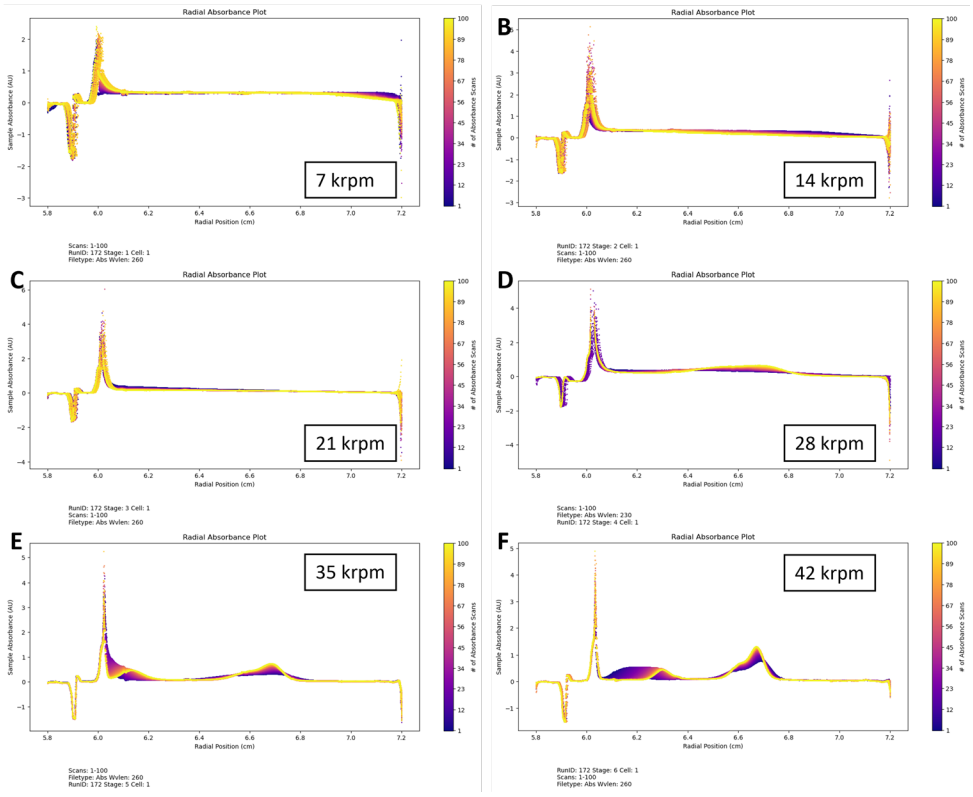

Table 4: Monitoring the effect of rotor speed on DGE-AUC of AAV in CsCl via a speed-step experiment. Data: Absorbance at 235 nm, 100 scans at 180 sec intervals for each rotor speed. A: 7 krpm, B: 14 krpm, C: 21 krpm, D: 28 krpm, E: 35 krpm, F: 42 krpm

This variation of rotor speed leads to changes in peak shape and location for the analyte, which is shown below in Figure 5 below. This is also an example of a plot generated by reading raw scan data into Origin as ASCII files and plotting. This is a very simple and quick workflow to implement. In the previous installment of this technical series "Fundamentals of Data Analysis", we had demonstrated a peak analysis workflow using Origin. This analysis is now repeated for the two of the plots shown in Figure 5 and the results tabulated below in Table 3.

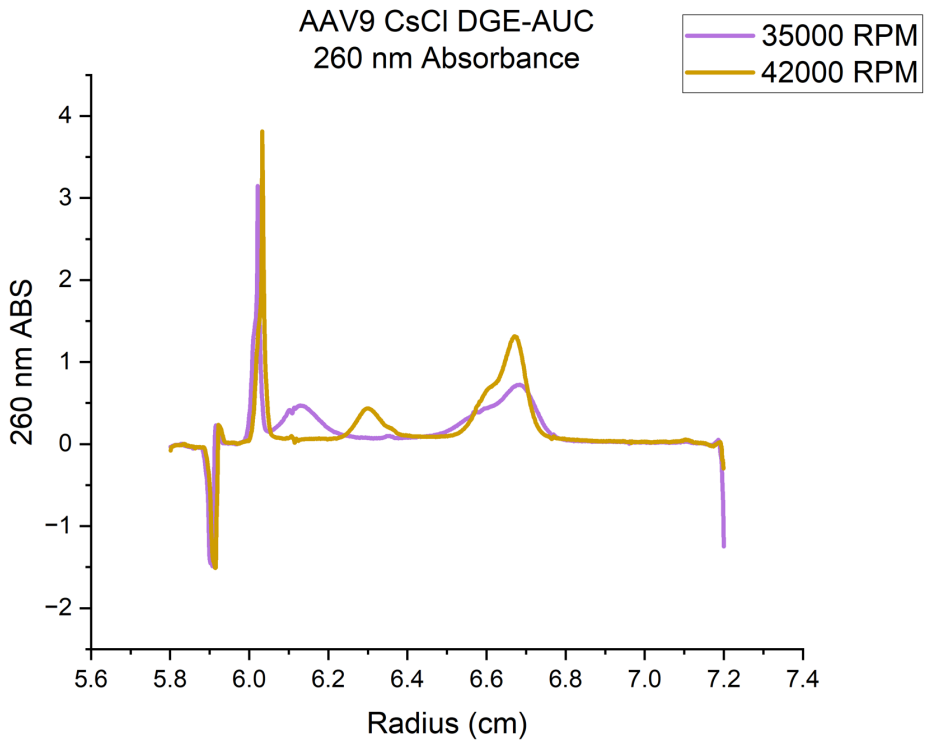

Figure 5: Variation of DGE-AUC absorbance curves for AAV at different rotor speeds

Expt Stage	Rotor Speed (krpm)	Peak #	Left Radius (cm)	Right Radius (cm)	Area	FWHM	Center	Height	Summed Area	% Area
6	42	1	6.23E+00	6.37E+00	1.85E-02	6.52E-02	6.30E+00	2.67E-01	1.12E-01	16.55
"	"	2	6.53E+00	6.76E+00	9.33E-02	8.81E-02	6.67E+00	9.58E-01		83.45
5	35	1	6.07E+00	6.20E+00	2.22E-02	8.37E-02	6.13E+00	2.71E-01	1.01E-01	21.99
"	"	2	6.50E+00	6.76E+00	7.86E-02	1.21E-01	6.69E+00	6.03E-01		78.01

Table 3: Results of peak analysis performed on AAV9 in CsCl DGE-AUC sample run at 35 krpm and 42 krpm rotor speeds

The following observations can be made:

1. The left and right limits for Peak #2, as autodetected by Origin peak analysis wizard are almost unchanged (6.53 to 6.76 cm).

2. The corresponding limits for Peak #1 are 6.07 to 6.20 cm at 35 krpm but are 6.23 to 6.37 cm at 42 krpm. Thus, Origin correctly detects that Peak #1 shifts inwards towards the isodensity point at higher rotor speed. This is also seen from the respective peak centers.

3. Both peaks are much wider at 35 krpm than at 42 krpm, as determined by full-width-at-half-maximum (FWHM): 28% more for Peak #1 and 37% more for Peak #2.

4. Interestingly enough, the height of Peak #1 actually drops slightly from 35 to 42 krpm, while it increases by almost 60% for Peak #2.

5. Finally, the percentage signal / population of Peak 1 drops from 21.9% at 35 krpm to 16.5% at 42 krpm, with the remainder of the signal attributed to Peak #2 at both speeds.

GFM Density Optimization

In the following example, we have performed DGE-AUC experiments on recombinant AAV9 capsids in a gradient of CsCl with PBS buffer at pH 7.4. Experiment conditions were as follows: 100 scans at a wavelength of 260 nm were collected, at intervals of 5 minutes. The experiment was carried out at a rotor speed of 42 krpm and at a temperature of 20°C. Figure 6 below shows the DGE peaks obtained with three different starting concentrations of CsCl, corresponding to densities of 1.37 g/ml (left panel A), 1.35 g/ml (middle panel B) and 1.33 g/ml (right panel C). The following observations can be made:

1. Equilibrium is attained for all three samples by the end of the experiment (~ 8 hrs).

2. The high density CsCl sample (1.37 g/ml) only shows only one large peak (with a shoulder) to the left of the pivot point. This corresponds to the majority population Peak #2 seen in Figures 4 and 5. This also suggests that the minority high density species which corresponds to Peak #1 in Figures 4 and 5 has now floated to the top of the cell and it is indistinguishable from the meniscus.

3. The low density CsCl sample (1.33 g/ml) also shows this large peak (with a less prominent shoulder) to the right of the pivot point. This is still identified as equivalent to Peak #2 in Figures 4 and 5. A small and broad peak is also visible near the pivot point/center, which is identified as equivalent to the minority Peak #1 in Figures 4 and 5.

4. The medium density CsCl sample (1.35 g/ml) shows the same large peak (with a shoulder), but this time somewhat sharpened. This is to the right of the pivot/isodensity point. The smaller peak is also seen, this time more prominent, to the left of the pivot point. This overall distribution is the same as in Figures 4 and 5.

This figure illustrates the importance of selecting the correct starting density for the GFM. Too high or too low of this starting density will lead to analyte species accumulating either in the meniscus or at the cell bottom. The correct density will show all analyte peaks, ideally separated around the pivot or isodensity point.

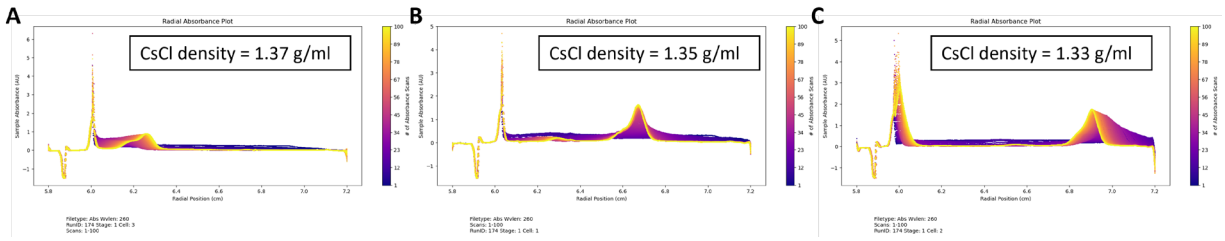

Figure 6: DGE-AUC of AAV in CsCl, A: CsCl density = 1.37 g/ml, B: CsCl density = 1.35 g/ml, C: CsCl density = 1.33 g/ml

Temperature Optimization

Experiment temperature has a significant effect on DGE curves. Lower temperature leads to less diffusion, resulting in sharper curves (all other parameters being equal). This effect is seen below in Figure 7, where we show the DGE curves for the AAV samples discussed previously with medium starting density of CsCl (1.35 g/ml). Experiment parameters were the same as mentioned for Figure 6,

with the exception of temperature. Panel A shows the DG curve at 20°C, while panel B is at 4°C. It can be seen that lowering the temperature leads to sharper and taller peaks. While this can be useful for samples with low analyte concentrations, it should also be noted that peak sharpening frequently results in loss of information about minority population species. This is seen in panel B vs panel A, where the curves at 4°C appear to not display the shoulder peak at 6.6 cm anymore.

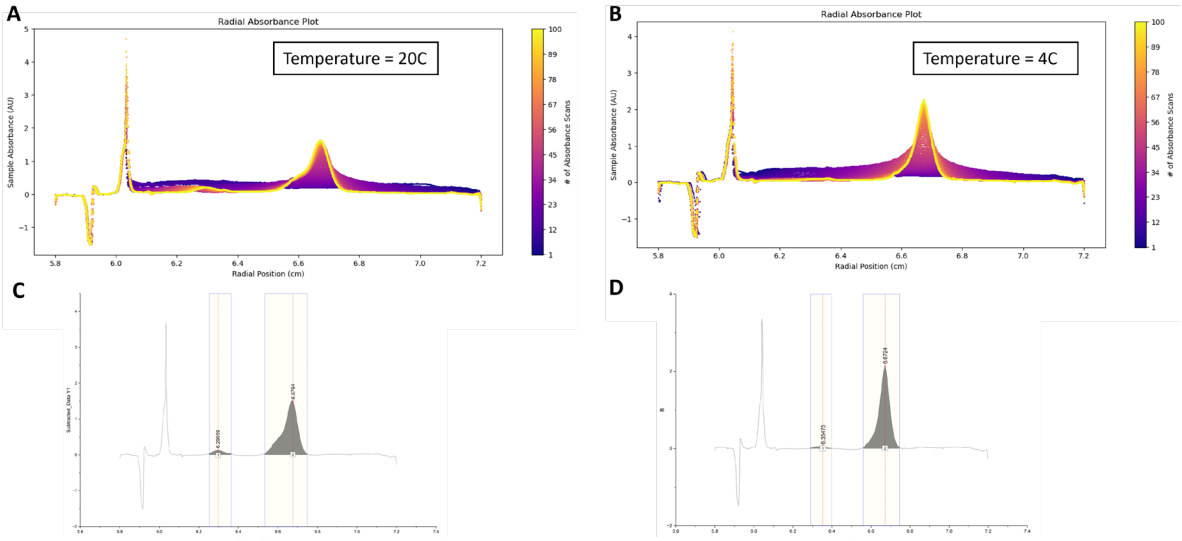

Figure 7: Effect of temperature in DGE-AUC of AAV in CsCl. A: Raw data at 20°C, B: Raw data at 4°C, C: Integration windows at 20°C, D: Integration windows at 4°C

Datasets from both experiments were subjected to peak analysis by Origin. The corresponding integration windows (after baseline adjustment) are shown in panels C and D for 20°C and 4°C respectively. The results of performing this peak analysis on the last scan (#100) for both experiments are tabulated below in Table 4.

Temp (°C)	Peak #	Left Radius (cm)	Right Radius (cm)	Area	FWHM	Center	Height	Summed Area	% Area
20	1	6.25E+00	6.36E+00	9.51E-03	6.77E-02	6.30E+00	1.36E-01	1.39E-01	6.83
"	2	6.53E+00	6.75E+00	1.30E-01	6.86E-02	6.67E+00	1.52E+00		93.17
4	1	6.29E+00	6.40E+00	4.25E-03	6.91E-02	6.35E+00	6.67E-02	1.41E-01	3.01
"	2	6.56E+00	6.75E+00	1.37E-01	5.40E-02	6.67E+00	2.15E+00		96.99

Table 4: Results of peak analysis performed on AAV9 in CsCl DGE-AUC sample run at 42krpm and 20°C and 4°C

The following observations can be made based on Table 4:

1. The population / signal percentage of Peak 1 changes from 6.83% at 20°C to 3.01% at 4°C. The remainder of the signal is attributable to Peak #2 (the large peak).

2. The center of Peak #1 shifts from 6.30 cm to 6.35 cm between 20°C to 4°C. The center of Peak #2 stays constant at 6.67 cm for both temperatures.

3. The height of Peak #1 decreases from 20°C to 4°C, while that of Peak #2 increases.

An additional point, not captured in Table 4 is that transiting from 20°C to 4°C reduces the left shoulder of Peak #2. As discussed previously, this shoulder may represent a minority population within Peak #2. This minority population now appears subsumed within the main body of Peak #2. Thus, reducing temperature may also change the relative populations of minority species.

Absorbance Optimization

The Optima AUC can record multiwavelength absorbance data[6]. This is useful for a mixture of samples which may contain analytes containing different chromophores (as will be discussed in the case study on liposomes). But it is also useful for an experiment with the same sample in different cells corresponding to a wide range of concentrations. Low concentration samples can be detected at a wavelength corresponding to higher signal absorption and vice versa. Care must be taken to choose wavelengths which do not saturate the absorbance detector (the detector limit is 3 absorbance units or AU). In the following experiment (carried out with the same conditions used in Figures 6 and 7 – using 1.35 g/ml of CsCl at 20°C), we have chosen the following wavelengths, which correspond to the following biochemical moieties[7-11]:

1. 230 nm (Panel A): Capsid protein peptide bonds as well as Mie scattering
2. 235 nm (Panel B): Shoulder of 230 nm peak
3. 260 nm (Panel C): DNA absorption
4. 280 nm (Panel D): Capsid protein aromatic sidechain absorption

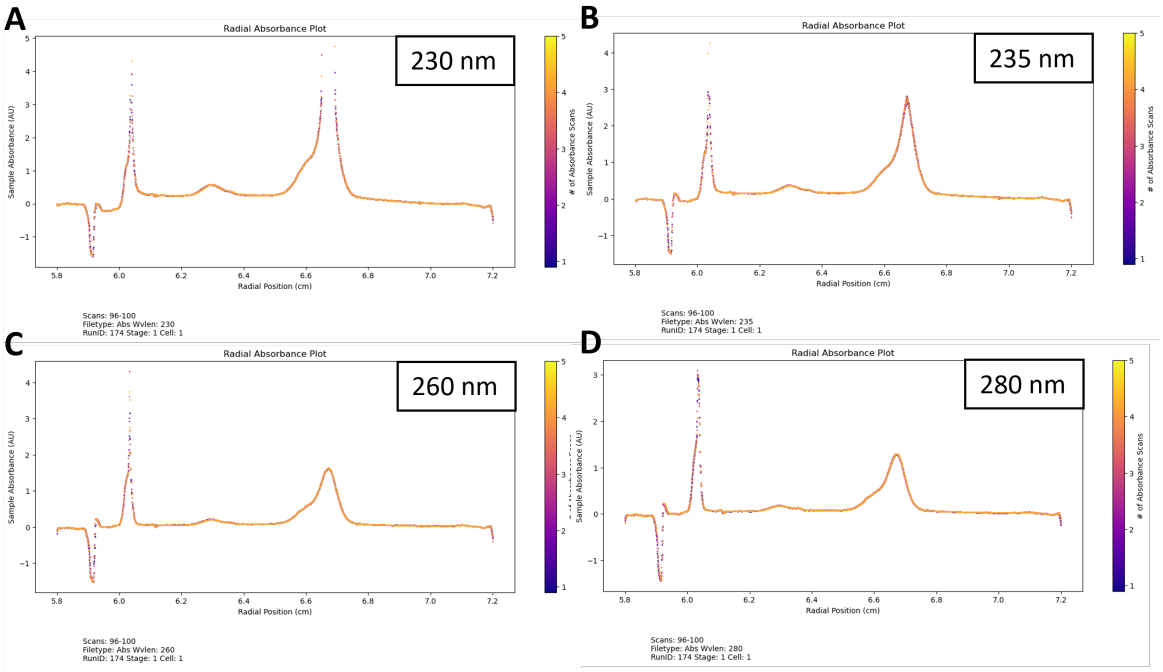

Figure 8: DGE-AUC of AAV in CsCl at different wavelengths. A: 230 nm, B: 235 nm, C: 260 nm, D: 280 nm

The results are shown above in Figure 8. We have plotted only the last 5 scans of the 100 scan experiment. We observe that:

1. The 230 nm peak has saturated the detector.
2. The other wavelengths are not saturated and can be used for peak quantification.
3. All wavelengths display overlapping scans – this indicates that the analyte has attained thermodynamic equilibrium.

Discussion and Conclusions

DGE-AUC separates analytes based on their buoyant density. This is orthogonal to the separation basis in the well-established techniques of Sedimentation Velocity or SV-AUC or Sedimentation Equilibrium or SE-AUC. Thus, DGE-AUC shows promise in providing an additional and valuable method to characterize and quantify different species in complex drug carrier systems (vectors) such as virus particles, nanoparticles and more[12-14].

As discussed in previous installments of this technical series, one of the attractive features of DGE-AUC is that it is easy and intuitive to visually interpret. Naturally, this means it is also easy to optimize DGE-AUC experiments based on visual inspection of data. We have showcased different types of experimental optimization to obtain superior DGE-AUC data in this application note.

Specifically, we show the following effects:

1. **Optimizing rotor speed:** higher speeds lead to larger density ranges sampled by the GFM. This leads to sample peaks that shift closer to the pivot or isodensity point and are also radially compressed. Lower speeds lead to smaller density ranges, which in turn lead to sample peaks that are shifted away from the isodensity point as well as resulting in lower peak heights and broader peaks overall. Thus, rotor speed must be adjusted to find a balance between peak separation (low speeds) and peak height or S/N ratio (higher speeds). When possible, multispeed, or speedstep experiments should be run. These will allow the user to track the movement of peaks with rotor speed and can provide the best compromise between peak separation and S/N.

2. **Optimizing GFM starting density:** low densities will lead to analytes accumulating at the cell bottom, while high densities will lead to analytes accumulating at the meniscus. Neither situation is desirable. Thus, it is recommended that the user try several different GFM starting densities, ideally in the same rotor/experiment.

3. **Optimizing temperature:** Lower temperatures lead to less diffusion, leading to taller and more radially compressed peaks. However, information about minority species which appear as shoulders to the main peak may be lost.

4. **Optimizing absorbance wavelength:** Two considerations apply here. The first is to select a wavelength corresponding to the biochemical moiety under study. The second is that detector saturation should be avoided. Since analysis of DGE-AUC experiments only requires the final few scans at equilibrium, it is possible to set up a multiwavelength experiment so that signal from some wavelengths is available for analysis even if others are saturated.

References

1. Cole, J. L. & Hansen, J. C. Analytical ultracentrifugation as a contemporary biomolecular research tool. J Biomol Tech 10, 163-176 (1999).

2. Meselson, M. & Stahl, F. W. THE REPLICATION OF DNA IN ESCHERICHIA COLI. Proc Natl Acad Sci U S A 44, 671-682 **https://doi.org/10.1073/pnas.44.7.671**

3. Grimm, D. & Büning, H. Small But Increasingly Mighty: Latest Advances in AAV Vector Research, Design, and Evolution. Hum Gene Ther 28, 1075-1086 (2017). **https://doi.org/10.1089/hum.2017.172**

4. Naso, M. F., Tomkowicz, B., Perry, W. L., 3rd & Strohl, W. R. Adeno-Associated Virus (AAV) as a Vector for Gene Therapy. BioDrugs 31, 317-334 (2017). **https://doi.org/10.1007/s40259-017-0234-5**

5. Santiago-Ortiz, J. L. & Schaffer, D. V. Adeno-associated virus (AAV) vectors in cancer gene therapy. J Control Release 240, 287-301 (2016). **https://doi.org/10.1016/j.jconrel.2016.01.001**

6. Beckman Analytical Ultracentrifuges, <https://www.beckman.com/centrifuges/analytical-ultracentrifuges/optima-auc> (2023).

7. Biter, A. B. et al. A method to probe protein structure from UV absorbance spectra. Anal Biochem 587, 113450 (2019). https://doi.org/10.1016/j.ab.2019.113450

8. Kattawar, G. W. & Plass, G. N. Electromagnetic scattering from absorbing spheres. Appl Opt 6, 1377-1382 (1967). https://doi.org/10.1364/AO.6.001377

9. Plass, G. N. Mie scattering and absorption cross sections for absorbing particles. Appl Opt 5, 279-285 (1966). https://doi.org/10.1364/AO.5.000279

10. Shen, C.-H. in Diagnostic Molecular Biology (Second Edition) (ed Chang-Hui Shen) 181-208 (Academic Press, 2023).

11. Van de Hulst, H. C. Light Scattering by Small Particles. (John Wiley and Sons, New York; Chapman and Hall, London., 1957).

12. Bepperling, A. & Best, J. Comparison of three AUC techniques for the determination of the loading status and capsid titer of AAVs. Eur Biophys J 52, 401-413 (2023). https://doi.org/10.1007/s00249-023-01661-0

13. Bepperling, A. & Richter, G. Determination of mRNA copy number in degradable lipid nanoparticles via density contrast analytical ultracentrifugation. Eur Biophys J 52, 393-400 (2023). https://doi.org/10.1007/s00249-023-01663-y

14. Savelyev, A., Brookes, E. H., Henrickson, A. & Demeler, B. A new UltraScan module for the characterization and quantification of analytical buoyant density equilibrium experiments to determine AAV capsid loading. Eur Biophys J 52, 311-320 (2023). https://doi.org/10.1007/s00249-023-01641-4

Legal Notices

For Beckman Coulter's worldwide office locations and phone numbers, please visit Contact Us at beckman.com

2024-GBL-EN-106823-v1